MIT Libraries | DSpace@MIT

MIT Open Access Articles

Inlet Flow Distortion in an Advanced Civil Transport Boundary Layer Ingesting Engine Installation

The MIT Faculty has made this article openly available. ***Please share*** how this access benefits you. Your story matters.

Citation: Hall, DK, Greitzer, EM, Uranga, A, Drela, M and Pandya, SA. 2022. "Inlet Flow Distortion in an Advanced Civil Transport Boundary Layer Ingesting Engine Installation." Journal of Turbomachinery, 144 (10).

Published Version: 10.1115/1.4054035

Publisher: ASME International

Permanent Link: https://hdl.handle.net/1721.1/145337

Version: Final published version: final published article, as it appeared in a journal, conference proceedings, or other formally published context

Terms of use: Article is made available in accordance with the publisher's policy and may be subject to US copyright law. Please refer to the publisher's site for terms of use.

Massachusetts Institute of Technology

Check for updates

D. K. Hall[1,2]
Department of Aeronautics and Astronautics,
Massachusetts Institute of Technology,
Cambridge, MA 02139
e-mail: david.k.hall@psu.edu

E. M. Greitzer
Department of Aeronautics and Astronautics,
Massachusetts Institute of Technology,
Cambridge, MA 02139
e-mail: greitzer@mit.edu

A. Uranga[3]
Department of Aeronautics and Astronautics,
Massachusetts Institute of Technology,
Cambridge, MA 02139
e-mail: auranga@usc.edu

M. Drela
Department of Aeronautics and Astronautics,
Massachusetts Institute of Technology,
Cambridge, MA 02139
e-mail: drela@mit.edu

S. A. Pandya
NASA Ames Research Center,
Moffett Field, CA 94035
e-mail: shishir.a.pandya@nasa.gov

Inlet Flow Distortion in an Advanced Civil Transport Boundary Layer Ingesting Engine Installation

This article presents first-of-a-kind measurements, and complementary computations, of the flow through the propulsion system of a boundary layer ingesting, twin-engine advanced civil transport aircraft configuration. The experiments were carried out in the NASA Langley 14- by 22-foot Subsonic Tunnel, using a 1:11 scale model of the D8 "double-bubble" aircraft with electric ducted fans providing propulsive power. Overall force and moment measurements and flow field surveys at the inlet and nozzle exit planes were obtained. The computations were carried out with the NASA OVERFLOW code. The measurements and computations were conducted for a range of aircraft angles of attack and propulsor powers representing operating points during the aircraft mission. Velocity and pressure distributions at the propulsor inlet and exit, and integral inlet distortion metrics, are presented to quantify the flow nonuniformity due to boundary layer ingestion. The distorted inflow exhibits qualitative and quantitative changes over the mission, from a unidirectional stratified stagnation pressure at cruise to a streamwise vortex structure at climb conditions. The computations capture these flow features and reveal the interactions between airframe and propulsor that create these three-dimensional flow variations.
[DOI: 10.1115/1.4054035]

Keywords: boundary layer ingestion, inlet distortion, propulsion-airframe integration, axial fan aerodynamics

1 Introduction

1.1 Boundary Layer Ingestion. In an aircraft with boundary layer ingestion (BLI), some fraction of the airframe boundary layer flows through the propulsor, i.e., the propeller or fan. The average propulsor inlet velocity is thus lower than the freestream velocity, which the propulsor would ingest without BLI, and the main benefit of BLI can be described based on this feature. For a given propulsor mass flow, the propulsive force imparted to the aircraft scales as the velocity increase, while the required power scales as the velocity increase squared. Hence, less propulsive power is required for a given propulsive force if the inlet velocity is lowered by BLI [1,2].

The aforementioned is by no means a complete explanation,[4] but it gives a qualitative description of the primary mechanism by which BLI reduces the required propulsive power and thus aircraft fuel burn. Calculations and detailed experiments have shown that, for the configuration described below, an 8–10% decrease in required power was achieved by ingesting 40% of the upper surface fuselage boundary layer[5] [4,5]. Other concepts seen in the literature include, for example, an axisymmetric propulsor mounted at the rear of a fuselage and ingesting the boundary layer from the whole fuselage [6,7]. The benefits of BLI are real and seem achievable, and a number of configurations are being investigated, at different levels of fidelity, to define guidelines and develop aircraft that integrate the airframe and the propulsor to take advantage of BLI [8–13].

Along with benefits, there are challenges created by BLI. For non-BLI aircraft, such as current civil transports, the flow into the propulsor has uniform stagnation pressure, and the turbomachinery sees a nominally axisymmetric flow with no large regions of appreciable radial nonuniformity. With BLI, the fan blades sweep through nonuniform fuselage boundary layer flow in each revolution, giving a circumferential and radial distortion that has the potential for detrimental aeromechanical and aerodynamic impact. For the former, the rotor is subjected to once-per-revolution forcing in incidence and velocity magnitude, including higher harmonics, that can excite blade resonances [14]. For the latter, the local (around the annulus) operating point of the rotor can sweep through regimes of low efficiency, or even stall conditions [15–17]. Further, the interaction between fan and nonuniform inflow can generate local swirl upstream of the fan, which impacts the unsteady variation in rotor incidence angle [18,19]. An aspect of this article is to describe and quantify the sources, and regimes of occurrence, of both types of distortion.

The nonuniform flow into the propulsor turbomachinery results from the interaction of the airframe and the engine, and this interaction can be conceptually separated into two categories. Upstream of the propulsor more than roughly one fan diameter, which we refer to as the *far-field*, the interaction is one-way downstream. In this region, the nonuniformities in stagnation pressure, streamwise vorticity, and other distortion parameters are determined mainly by the aircraft operating condition. The nonuniformities depend only weakly on engine operating point, and, if a dependence exists, it

[1]Corresponding author.
[2]Present address: Department of Aerospace Engineering, The Pennsylvania State University, University Park, PA 16802.
[3]Present address: Department of Aerospace and Mechanical Engineering, University of Southern California, Los Angeles, CA 90089.
[4]More precisely, neither mass flow nor force are necessarily the same, and there are other favorable consequences than those arising from the reduction in inlet velocity [2–4].
[5]This is the *aerodynamic benefit* only. There is also a roughly equivalent benefit from other system-level effects.

Contributed by the International Gas Turbine Institute (IGTI) of ASME for publication in the Journal of Turbomachinery. Manuscript received December 25, 2021; final manuscript received January 18, 2022; published online April 7, 2022. Tech. Editor: David G. Bogard.

This work is in part a work of the U.S. Government. ASME disclaims all interest in the U.S. Government's contributions.

Downloaded from http://asmedigitalcollection.asme.org/turbomachinery/article-pdf/144/10/101002/6870956/turbo_144_10_101002.pdf by Massachusetts Inst Of Tech. user on 09 September 2022

is one-dimensional, that is to say due to the overall mass flow through the propulsor. Closer to the propulsor, in the *near-field*, however, the velocity field depends in a major way on local static pressure field nonuniformities resulting from the nonuniform pressure rise response of the turbomachinery to the distorted inlet flow [18,19].

For low hub-to-tip ratio fans, as in civil transport engines, BLI inlet distortion typically includes circumferential and radial nonuniformities in pressure, axial velocity, and swirl, and depends on both engine and aircraft operating conditions, as shown in Sec. 4. The upstream interaction due to the turbomachinery is well known for stagnation pressure distortion—see, for example, Refs. [15,19,20]—but has not been defined in depth for the combined stagnation pressure and streamwise vortical distortions encountered with BLI.

1.2 Aircraft Configuration Examined. The aircraft configuration examined is the D8, shown in Fig. 1. The D8 was designed for the single-aisle transport market, with a design payload of 180 passengers and design range of 3000 nautical miles. Aspects of the configuration, including the *double-bubble* lifting fuselage and BLI, were chosen for minimum mission fuel consumption. The aircraft has two propulsors next to each other inboard of twin vertical tails at the rear of the upper fuselage surface. The fuselage carries approximately 19% of the aircraft lift at cruise, compared to 14% in a conventional transport aircraft. At cruise conditions, the propulsors ingest approximately 40% of the fuselage boundary layer, with a boundary layer thickness of roughly half a fan diameter [10,11].

1.3 Scope of the Paper. This article uses both wind tunnel measurements and computations to show the features of BLI distortion and the mechanisms of generation. The measurements were made on a 1:11-scale powered model of the D8. The computations link the measurements to the fluid dynamic processes that create the fan distortion, to connect *what* happened with *how* the features of the inlet distortion arise and *why* they look the way they do. The measurements and computations were carried out for different operating points (angle of attack and propulsive power) that represent a typical transport mission. To our knowledge, they are first-of-a-kind reports on the distortion features, and they show qualitative and quantitative changes in inlet distortion with aircraft angle of attack, from an approximately vertically stratified inlet stagnation pressure nonuniformity at simulated cruise (2 deg angle of attack) to an embedded streamwise vortex at high angle of attack (8 deg).

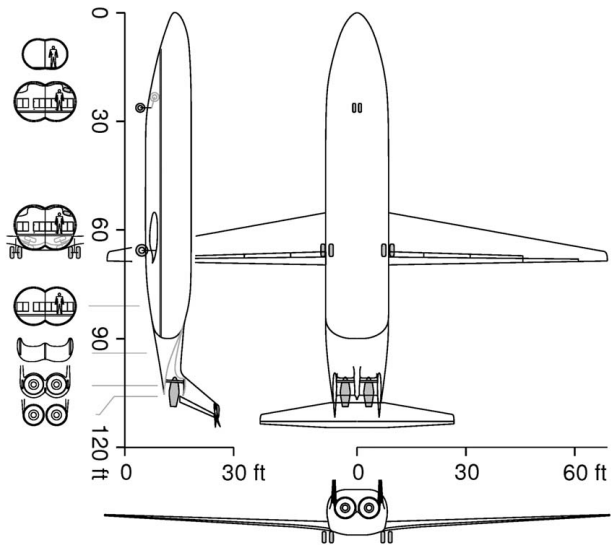

Fig. 1 Three-view of the D8 advanced civil transport aircraft [21]

Information is also provided on the *distortion transfer*, i.e., the relation between exit and inlet distortions. Integral distortion properties are presented in terms of a standard parameter used to correlate engine response to inlet distortion, to provide a measure of the BLI distortions at different mission conditions.

This article is organized as follows. Section 2 describes the methodology, including the facility, experimental setup, and computational procedure. Section 3 gives detailed results for the simulated cruise condition, including the inlet flow field, distortion transfer, and streamwise evolution of the ingested flow; the applicability of the computational propulsor model is also discussed. Section 4 illustrates variations in inlet distortion and mechanisms of distortion generation with aircraft operating condition and provides quantification of the measured distortions using an integral distortion metric. A summary and conclusions are presented in Sec. 5.

2 Methodology

2.1 Experimental Setup and Data Acquired. The experiments were carried out at the NASA Langley 14- by 22-foot Subsonic Tunnel, on a 1:11 scale (4.1 m wingspan) D8 aircraft model with electric ducted fans to provide propulsive power. The fan diameter was 14.6 cm. The maximum freestream Mach number was 0.11 and so the flow can be considered incompressible. The geometric model blockage was 0.5%, and no wall corrections have been applied. The Reynolds number based on average wing chord ranged between 3.6×10^5 and 6.8×10^5, and the model was outfitted with boundary layer trip strips on the wing, tails, and fuselage nose to better represent the fully turbulent flow expected at full-scale Reynolds numbers [21].

For a given tunnel speed and propulsor nozzle geometry,[6] setting an operating point required fixing two parameters: *aircraft angle of attack*, α, and *propulsor power*, controlled through the ratio of fan rotational speed to freestream velocity, $\Omega r_{\text{tip}}/V_\infty$. The simulated cruise condition was defined as 2 deg angle of attack and *zero net streamwise force* on the model, as measured by the tunnel balance. For other conditions, the operation was determined by setting the angle of attack and fan power to obtain predetermined values of net streamwise force coefficient, $C_X = F_X/(0.5\rho V_\infty^2 S_{\text{ref}})$, and total stream-normal force coefficient, $C_Z = F_Z/(0.5\rho V_\infty^2 S_{\text{ref}})$, where F_X and F_Z are the axial and vertical components of force, respectively, in the wind tunnel coordinate system.[7]

In traditional aircraft performance analysis, the total streamwise force is computed as F_X = Drag – Thrust. In the present experiment, we do not decompose the measured force into contributions from thrust and drag, and F_X is instead measured *directly*, for two reasons: first, appropriate definitions of drag and thrust are ambiguous in the presence of BLI, and second, the streamwise force F_X is well defined and measurable, and it alone is sufficient to determine whether the aircraft climbs, descends, or is in level flight. For similar reasons, the total stream-normal force, F_Z, was also measured directly.

The measurements included forces and moments on the model, fan rotation speed, motor electrical power, and flow surveys on planes upstream and downstream of the propulsor inlet and downstream of the nozzle exit. The results showed an 8.2% reduction in cruise propulsive power (the power needed to obtain $F_X = 0$), relative to a non-BLI model configuration. Further information about the model, wind tunnel facility, test program, and measured BLI benefit is given in Refs. [4,5,21].

Flow surveys, made using five-hole probes, provided information on the three velocity components and the static and stagnation pressure at propulsor inlet and exit. The surveys were conducted using a

[6]Multiple nozzle geometries were used to vary propulsor mass flow and propulsive efficiency [4]. We present results here for a single nozzle area.

[7]The aforementioned assumes that yaw angle is zero. A few measurements were carried out at non-zero yaw, and these required also setting the yaw angle.

Downloaded from http://asmedigitalcollection.asme.org/turbomachinery/article-pdf/144/10/101002/6870956/turbo_144_10_101002.pdf by Massachusetts Inst Of Tech. user on 09 September 2022

Fig. 2 Boundary layer ingesting ducted fans integrated into D8 wind tunnel model empennage with five-hole probe inlet traverse system (photo credit: NASA/George Homich)

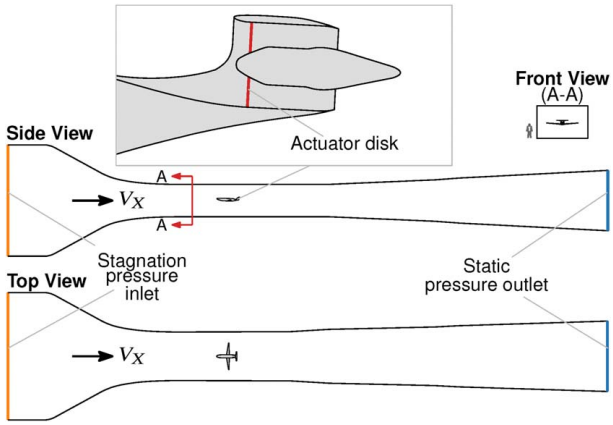

Fig. 4 Computational domain: three views of wind tunnel contraction, test section, and first diffuser; propulsive power modeled by uniform static pressure rise actuator disk (inset)

two-degree-of-freedom traverse system shown in Figs. 2 and 3. A drilled elbow probe, 175 mm long with an L-shaped probe head 4 mm long and 1.59 mm in diameter (custom-made by Aeroprobe Corporation), was used at the inlet plane, and a straight, 152 mm long, 3.18 mm diameter probe (Aeroprobe Corporation model PS5-C318-152) was used at the nozzle exit plane. Probe calibration for velocities between 10 and 40 m/s and probe-relative flow angles up to 60 deg were provided by the manufacturer. For angles larger than approximately 45 deg, the stagnation point on the probe approaches the side hole locations, causing errors when using the calibration, and results for flow angles greater than 40 deg are not reported. The small regions in which this occurred account for less than 2% of data points; these appear as white areas near the vertical tails in the contour plots in Figs. 13, and 14. The probe measurements are accurate to within ±1 deg in flow angle and 3% in stagnation pressure coefficient.

The probes were installed on traverse systems with two rotating arms, whose angular positions were controlled by two stepper motors with parallel rotation axes. This allowed accurate placement of the probes on planes at the inlet and exit of the propulsor. Two versions of the system were constructed to obtain data at the planes indicated by vertical lines in Fig. 3. The traverse system support was mounted to the wind tunnel model support. Supports fixed to the nacelle for the inlet traverse, and to the horizontal tail for the nozzle exit traverse, ensured that the measurement plane was normal to the aircraft model axis, independent of model orientation. The inlet measurement plane was 8% of the fan diameter forward of the highlight of the propulsor inlets, corresponding to 19% of the fan diameter forward of the fan leading edge, and the nozzle exit measurement plane was 8% of the exit nozzle diameter aft of the nacelle trailing edge.

Figures 3(*b*) and 3(*c*) show the measurement point grids at inlet and exit planes. At the simulated cruise condition, each propulsor had 910 inlet measurement points, with higher resolution in the lower half of the flow annulus to resolve the fuselage boundary layer. The nozzle exit plane survey consisted of 943 points. For conditions other than cruise, only inlet measurements were collected; measurements at different aircraft angles of attack had a coarser grid of 516 points for both propulsor inlets, and measurements at different propulsor power at high angle of attack (8 deg) had a grid of 952 points.[8]

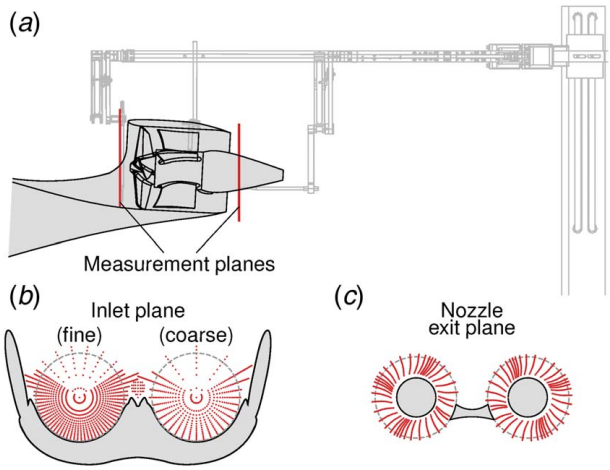

Fig. 3 (*a*) Model-mounted survey systems and measurement plane locations, (*b*) measurement grids for BLI inlet, and (*c*) nozzle exit surveys

2.2 Computational Approach. Full aircraft calculations were carried out using the NASA OVERFLOW Reynolds-averaged Navier–Stokes code [22]. The code uses second-order central differencing discretization with matrix dissipation smoothing, low Mach number preconditioning, and the Pulliam–Chaussee diagonalized approximate-factorization implicit solution algorithm [23]. Fully turbulent flow was assumed in the computations, consistent with the use of trips near the leading edges of the model surfaces. The k-ω shear stress transport turbulence model [24] was used.

The flow domain, shown in Fig. 4, included the wind tunnel test section and the aircraft model. The internal propulsor flow was represented using an actuator disk inside the nacelle, axially located at approximately the propulsor rotor mid-chord, indicated by the vertical line in the inset view of the propulsor in Fig. 4. The description imposes a uniform static pressure rise across the actuator disk, while also satisfying continuity, and with no change in the velocity components in the plane of the disk. The pressure rise was adjusted to achieve a specified net aircraft streamwise force coefficient, C_X. The mesh was an overset grid with approximately 141 million points, and a y^+ of unity or less on all solid surfaces. Half the geometry was modeled, with a symmetry of plane boundary condition. Single-point solutions were achieved on average in 200 CPU-hours on 600 Haswell CPU nodes on the NASA Pleiades supercomputer. The grid generation and solution processes are described in Refs. [25,26].

[8]Higher resolution inlet and exit data were required for the assessment of the mechanical flow power [21]; the coarser inlet measurements are still sufficient to resolve BLI inlet flow features and define appropriate inlet distortion metrics.

Downloaded from http://asmedigitalcollection.asme.org/turbomachinery/article-pdf/144/10/101002/6870956/turbo_144_10_101002.pdf by Massachusetts Inst Of Tech. user on 09 September 2022

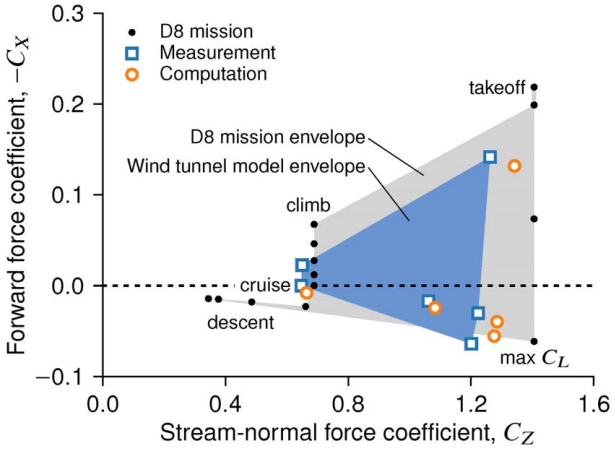

Fig. 5 Aircraft operating conditions: forward force coefficient, $-C_X$, versus stream-normal force coefficient, C_Z; full-scale aircraft mission, wind tunnel model, and computational operating points

2.3 Aircraft Operating Conditions. The measurements and CFD calculations were carried out for operating conditions encountered during a transport aircraft mission. The conditions are shown in Fig. 5 for a full-scale aircraft and for the wind tunnel model. The horizontal axis is the stream-normal force coefficient, C_Z, corresponding to the lift coefficient, and the vertical axis is the forward force coefficient, i.e., the coefficient of force in the direction of simulated flight, $-C_X$, which is positive during climb, negative during descent, and zero in level cruise. Compared to cruise, C_Z is reduced during descent and increased at takeoff, cutback, start of climb, and approach at high lift. The lightly shaded area denotes the full-scale aircraft operating conditions, and the darker shaded area denotes the wind tunnel model operating envelope. The open squares indicate the measurement points, and the open circles indicate the CFD computations.

The C_X and C_Z values were obtained in experiments without the survey system installed [5,21]; the propulsor surveys were taken separately at the same freestream velocity, angle of attack, and fan angular speed. The maximum measured C_Z was limited by the stiffness of the model support to about 1.1 at an angle of attack of 8 deg. The most negative measured C_X was limited by the fan power at which the internal motor temperature reached its limit; the most negative calculated C_X was limited by a numerical instability in the jet shear layer at high power. In addition to points at the corners of the operating envelope, to assess effects of the airframe and propulsor on propulsor inlet distortion, surveys were taken at multiple angles of attack for fixed fan speed and multiple fan speeds for the fixed angle of attack.

In the full aircraft computations (open circles in Fig. 5), variation in angle of attack at fixed propulsor fan pressure rise corresponds approximately to measurements at constant nondimensional fan rotation speed, $\Omega r_{tip}/V_\infty$, and variation in propulsor fan pressure rise at constant angle of attack corresponds to variations in nondimensional rotation speed at constant angle of attack. The computed C_Z is 6% higher than the measurements at the highest angle of attack, but the solutions exhibit the features observed in the experiment (see Sec. 4).

3 Flow Field for Simulated Cruise Condition

3.1 Inlet Distortion. Figure 6 shows measured and computed distributions of inlet stagnation pressure coefficient, static pressure coefficient, and vertical and spanwise flow angles at the simulated cruise condition. The computed flow field is symmetric, and only the right-hand side (aft looking forward) is shown. The measurement and computation plane is indicated by the upstream vertical

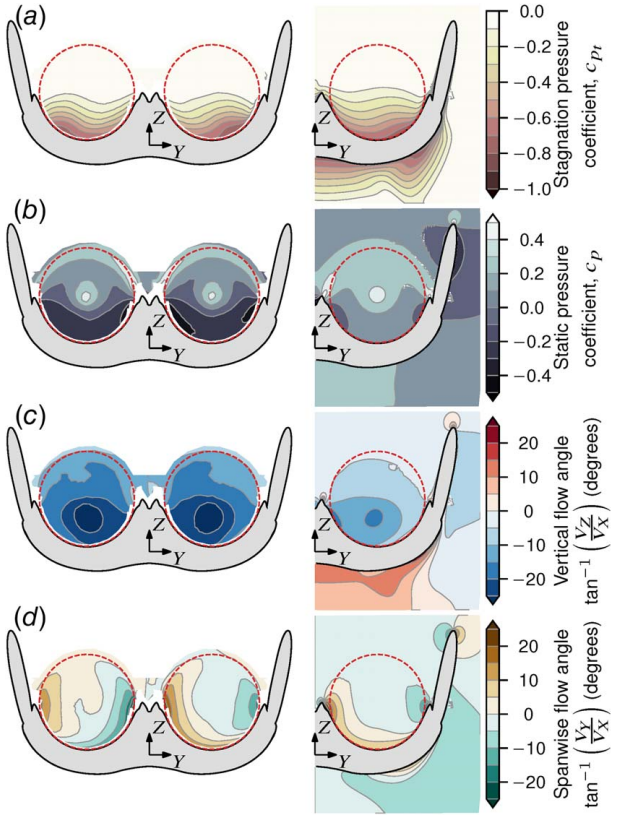

Fig. 6 Measured (left) and computed (right) cruise inlet (*a*) stagnation pressure coefficient, (*b*) static pressure coefficient, (*c*) vertical flow angle, and (*d*) spanwise flow angle

line in Fig. 3; the fuselage and vertical tail cross section at that location are indicated by the gray shaded area, and the circumference of the tip of each fan is indicated by the dashed lines in Fig. 6. For the measurements, the extent of the contours is limited to the interior of the survey area. For the computations, contours outboard of the vertical tails and below the fuselage are also shown to provide a context of the overall aircraft flow field.

At the simulated cruise condition, the stagnation pressure distribution is close to vertically stratified, consistent with planar boundary layer development over the top of the fuselage. The flow angles indicate the ingested streamtube contracts as it approaches the propulsor, with negative vertical (Z-direction) velocities and spanwise (Y-direction) velocities pointed toward the center of each propulsor.

The lower static pressure coefficient over the bottom half of the fans (Fig. 6(*b*)) and negative Z-velocity (Fig. 6(*c*)) are consistent with a top-to-bottom flow redistribution due to larger acceleration of the low momentum boundary layer fluid. In the rotor-relative frame, the negative Z-velocity results in fan rotor incidence variation from local co- and counter-swirl, in addition to incidence variation from the axial velocity nonuniformity [15,20]. The propulsors on the D8 have a low offset with respect to the fuselage (see Figs. 1 and 2) and small streamline curvature in the spanwise-normal plane; the two counter-rotating streamwise vortices that characterize BLI with higher offset [27] are thus not present.

Figure 7 shows the difference between the measured and computed distributions of the quantities in Fig. 6 over the fan inlet area. There is good agreement in the magnitude of the boundary layer stagnation pressure loss and the shape of the stagnation pressure distortion, with differences between measured and computed stagnation pressure coefficient of less than 0.1 over most of the inlet. There is qualitative agreement in the top-to-bottom flow redistribution, but the computations overestimate the static pressure and the vertical flow angle near the bottom of the fan and underestimate

Downloaded from http://asmedigitalcollection.asme.org/turbomachinery/article-pdf/144/10/101002/6870956/turbo_144_10_101002.pdf by Massachusetts Inst Of Tech. user on 09 September 2022

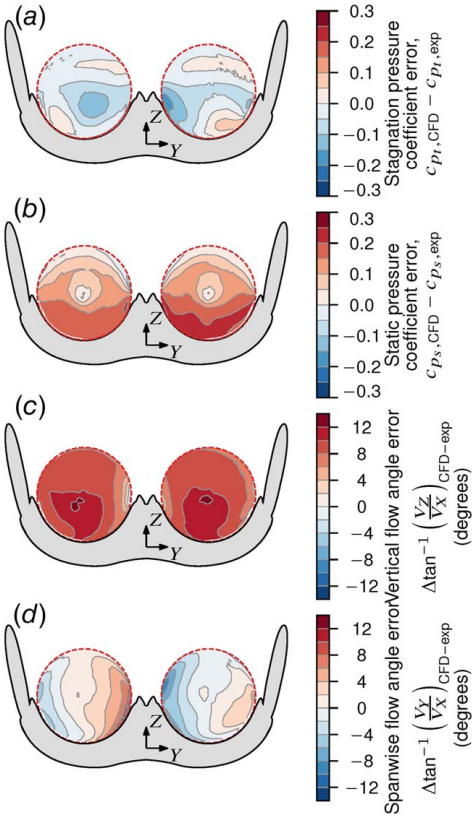

Fig. 7 Difference between measured and computed cruise inlet (*a*) stagnation pressure coefficient, (*b*) static pressure coefficient, (c) vertical flow angle, and (*d*) spanwise flow angle

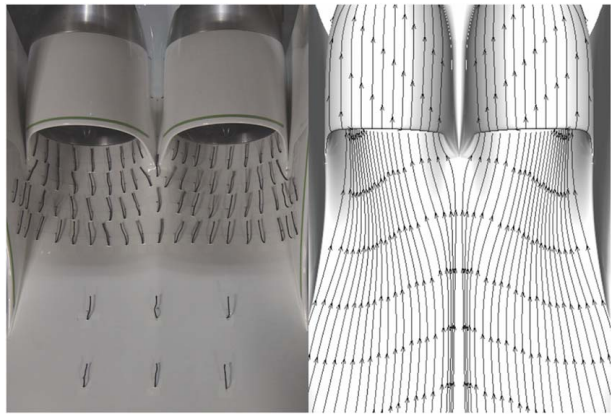

Fig. 8 Aft fuselage surface streamlines at simulated cruise condition: wind tunnel model tufts (left) [5] and computed surface streamlines (right)

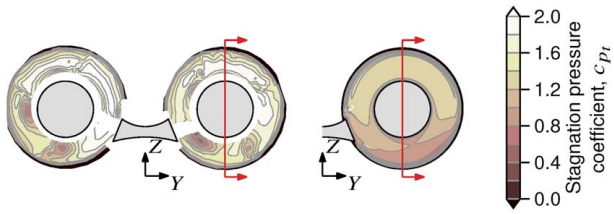

Fig. 9 Measured (left) and computed (right) cruise nozzle exit stagnation pressure coefficient

the spanwise streamtube contraction. The differences are mainly due to the approximation of uniform pressure rise across the actuator disk, which results in a smaller variation in inlet static pressure than in the actual flow, so the strength of the top-to-bottom flow redistribution is underestimated, leading to the 5 deg–10 deg difference in the vertical flow angle between measurements and computations. We discuss the limitations of the uniform pressure rise approximation in Sec. 3.3.

Figure 8 provides information about the surface flow pattern entering the propulsors. The image on the left shows tufts attached to the model to indicate the flow direction near the surface, and the image on the right shows computed surface streamlines. Both indicate flow migration away from the strake separating the two propulsors, consistent with the measured spanwise flow angles near the bottom of the fans.

For co-rotating fans with the same angular speed, the symmetric inlet spanwise flow creates a difference in rotor incidence between the two fans. For fans with clockwise rotation (aft looking forward), the left fan experiences co-swirl and a *reduction* in incidence near the fuselage surface, while the right fan experiences counter-swirl and an *increase* in incidence. This effect is evident from the asymmetry in measured static pressure in Figs. 6(*b*) and 7(*b*). In the wind tunnel experiments, this was manifested as a difference in power between the two fans at equal angular speed due to the increased pressure rise of the right-hand fan [5]. This effect also has implications for differences in efficiency, operability, and unsteady force between the two fans.

3.2 Fan Distortion Transfer. We now examine conditions at the nozzle exit, which provide insight into fan distortion response and distortion transfer, specifically attenuation of stagnation pressure distortion by the fan. Figure 9 shows the measured and computed nozzle exit stagnation pressure coefficient at the simulated cruise condition. The measurement and computation plane is indicated by the downstream vertical line in Fig. 3.

There are two principal differences between the measured and computed distributions. One is the areas of low stagnation pressure due to stator vane wakes and corner vortices, seen in the measurements, but not the computations. The reason for the difference is that the actuator disk model smears out the effect of the vanes and does not describe the discrete vane wake structure. The second difference is that the nonuniformity in stagnation pressure, outside the vane wakes and end wall boundary layers, is larger in the computation than the measurements; the difference is roughly 20% of freestream dynamic pressure.

The stagnation pressure distortion at inlet and exit is illustrated more directly in Fig. 10, which shows the radial stagnation pressure distribution at fan inlet and nozzle exit measurement planes for the right-hand propulsor. The horizontal axis is the stagnation pressure coefficient, and the vertical axis is nondimensional distance along the vertical diameter, with 0 at the fan axis and ±1 corresponding to fan top and bottom. At the exit station, the flow annulus covers from roughly ±0.5 at the wall of the center body to ±1.0 at the nozzle trailing edge. The solid lines are measurements, and the dashed lines are computations.

To illustrate the distortion transfer, we have indicated in the figure the difference in measured nozzle exit stagnation pressure of the upper and lower parts of the annulus, at the points outside the end wall boundary layers, as the horizontal line, $\Delta c_{p_t\mathrm{exit}}$. We have also marked the difference between freestream and inlet boundary layer stagnation pressure at approximately the same radial location, $\Delta c_{p_t\mathrm{inl}}$. Comparison of the measured exit and inlet stagnation pressures shows that the difference has been reduced because the low stagnation pressure flow undergoes a larger stagnation pressure increase than does the high stagnation pressure flow. The fan thus attenuates the distortion, resulting in a smaller

Downloaded from http://asmedigitalcollection.asme.org/turbomachinery/article-pdf/144/10/101002/6870956/turbo_144_10_101002.pdf by Massachusetts Inst Of Tech. user on 09 September 2022

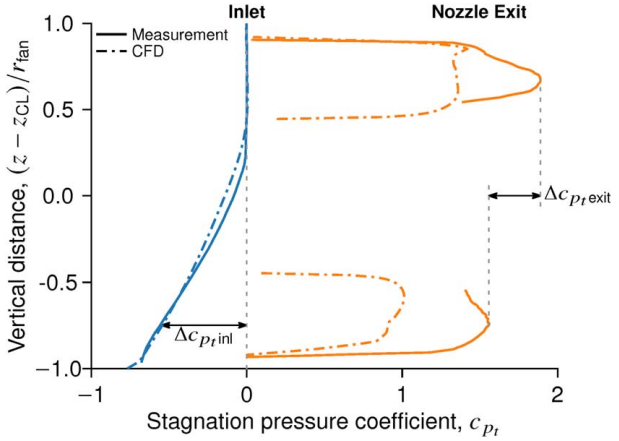

Fig. 10 Measured and computed inlet and nozzle exit stagnation pressure coefficient on vertical cut through the propulsor centerline (indicated in Fig. 9)

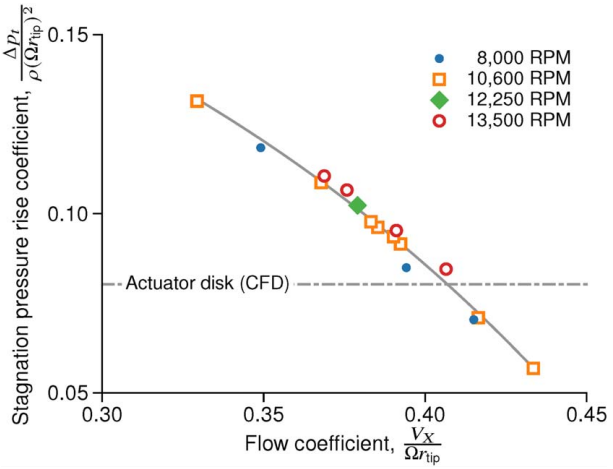

Fig. 11 Measured stagnation pressure rise coefficient versus flow coefficient for the electric ducted fan propulsor simulators; comparison with equivalent uniform pressure rise characteristic implemented in the computations

nonuniformity at fan exit. In the computations, however, the actuator disk provides the same stagnation pressure rise for all locations in the annulus,[9] and the nonuniformity is unchanged.

3.3 Suggestions for an Improved Distortion Attenuation Description. It is useful to probe deeper into distortion attenuation as a springboard for the explanation of the behavior and to highlight features of the modeling that should be incorporated in future analyses. The present fan description was used because it made the least demands on the information needed about the way in which the fan processes the nonuniform flow. To improve on this description, we need to include an additional effect, namely, linking the changes in local fan pressure rise to the local dynamic pressure and flow angle. The arguments start from the generic fan behavior that, for a given rotation rate, the pressure rise decreases with the increasing axial velocity. This is illustrated, for the propulsors used in the experiments, in Fig. 11, which shows the nondimensional pressure rise coefficient, $\Delta p_t/[\rho(\Omega r_{tip})^2]$, versus flow coefficient, $V_X/(\Omega r_{tip})$, for four angular speeds, measured in separate experiments to characterize propulsor performance [28]. Extending this idea to nonaxisymmetric inlet flow, if we assume each streamline through the fan operates locally on the pressure rise characteristic,[10] the implication is that the pressure rise is larger where the inlet stagnation pressure and velocity are lower, and the stagnation pressure distortion is thus attenuated by the fan.[11]

The aforementioned behavior also implies an upstream flow redistribution associated with inlet distortion. Suppose there is parallel exit flow with no swirl at the fan exit, so the exit static pressure is uniform. The variation in pressure rise just described means that, at fan inlet, the static pressure is lower than the average in the low velocity region and higher than the average in the high velocity region. Far upstream (beyond the near-field), however, there is no upstream influence of the fan. In the upstream near-field, therefore, there is acceleration in low stagnation pressure streamtubes and deceleration in high stagnation pressure streamtubes, and, for BLI type distortions, a top-to-bottom flow redistribution. As with distortion attenuation, the uniform pressure rise fan model does not describe this effect and will thus underestimate the inlet static pressure nonuniformity and flow angles (Fig. 6).

[9]The flow is effectively incompressible, and a uniform static pressure rise with no velocity change across the disk results in a uniform stagnation pressure rise.

[10]This approximation, known as parallel compressor theory, is a well-developed approach to nonaxisymmetric flow in compressors, which serves to give useful qualitative, and often quantitative, descriptions of compressors and fans with inlet distortion.

[11]In contrast, if there were a constant pressure rise across the fan regardless of inlet velocity, as represented by the dashed horizontal line in Fig. 11, the distortion magnitude would be the same at the exit as at the inlet.

The differences between measured and calculated distortion response point up to requirements for additional accuracy in modeling BLI propulsors in integrated vehicle computations. The propulsor affects the upstream flow redistribution for the fan, so velocities and flow angles at the fan face calculated using uniform pressure rise or constant static pressure outflow boundary conditions cannot provide appropriate conditions at the turbomachinery leading edge. Improved propulsor models such as actuator disks with velocity-dependent pressure rise, or body force methods, which replicate realistic blade row performance, should improve prediction of these flow features with little or no additional computational cost [2,20,29].

As a final comment on this topic, we emphasize that the limitations of the current description mainly affect the near-field effects of fan–distortion interaction and distortion transfer. More than roughly a diameter upstream of the fan, there should not be a substantial effect on the external flow aerodynamics. This statement is supported by the good agreement, qualitative and quantitative, between measured and computed inlet stagnation pressure in Fig. 6; the fuselage boundary layer develops over a much longer distance than the length scale of influence of the propulsor, and the boundary layer loss and streamline pattern are not appreciably modified by the fan–distortion interaction effects. Hence, we limit the remaining analysis to characterization of the far-field flow behavior, the inlet stagnation pressure, and the inlet streamwise vorticity.

3.4 Upstream Ingested Streamtube Behavior. Figure 12 shows computed propulsor capture streamtubes on the aircraft fuselage at the simulated cruise condition. The shaded areas indicate the streamtube cross sections at axial locations along the aircraft, with the heavy dark lines showing the streamtube boundaries. The figure illustrates the three-dimensional nature of the upstream flow and the spanwise (y-direction) contraction of the streamtubes as they near the inlet. The fluid that is ingested comes from under the nose and then moves around the sides of the fuselage. As the streamtubes approach the propulsor and respond to its pressure field, they increase in height and decrease in spanwise extent, as seen in the final six streamtube cross sections upstream of the propulsor. Additional aspects of evolution of the ingested boundary layer at different operating conditions is shown in Sec. 4.3.

4 Inlet Distortions at Noncruise Conditions

4.1 Effect of Angle of Attack on Stagnation Pressure Distortion. Figure 13 shows measured and computed inlet

Downloaded from http://asmedigitalcollection.asme.org/turbomachinery/article-pdf/144/10/101002/6870956/turbo_144_10_101002.pdf by Massachusetts Inst Of Tech. user on 09 September 2022

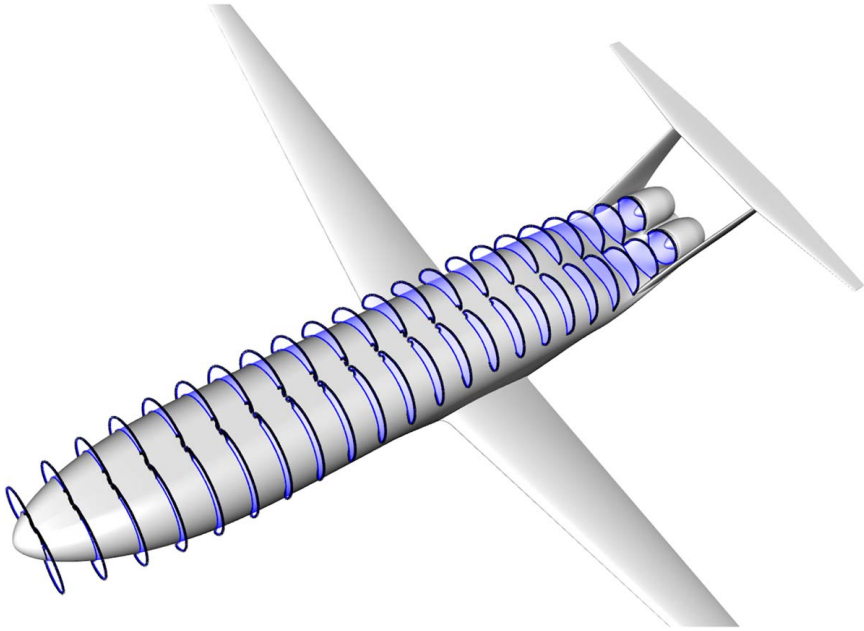

Fig. 12 Computed propulsor flow capture stream tube (image credit: NASA/Tim Sandstrom)

stagnation pressure coefficient distributions at $\Omega r_{tip}/V_\infty = 2.7$, the cruise fan speed, for aircraft angles of attack of 2, 6, and 8 deg. The quantitative differences in the measured and computed forces (Fig. 5) and the inlet stagnation pressure distribution are larger than at the simulated cruise condition. The computations, however, describe the peak-to-peak variation in stagnation pressure and relative changes in the shape of the distortion with changes in the angle of attack, and they provide useful insight into the qualitative behavior of the ingested distortion at off-design conditions. For the larger angles, the inlet distortion is no longer vertically stratified and shows vortical structures with scale comparable to the fan diameter. The minimum stagnation pressure coefficient is similar for all the cases, suggesting that the change with the angle of attack is mainly an inviscid alteration in streamline shape; the viscous losses over the length of the fuselage are similar, and the shape of the ingested boundary layer is altered by the increased streamwise vorticity generated at larger angles of attack.

4.2 Effect of Fan Power Level on Stagnation Pressure Distortion. For the D8 mission, the largest variations in propulsor power occur at higher angles of attack and C_Z. We therefore

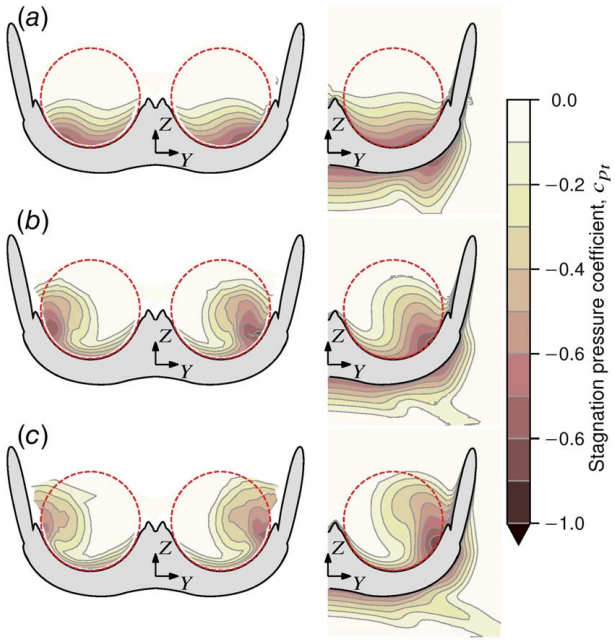

Fig. 13 Effect of angle of attack on inlet stagnation pressure distortion: measured (left) and computed (right) inlet stagnation pressure coefficient at simulated cruise fan speed (measurements) or pressure rise (computations): (*a*) $\alpha = 2$ deg, (*b*) $\alpha = 6$ deg, and (*c*) $\alpha = 8$ deg

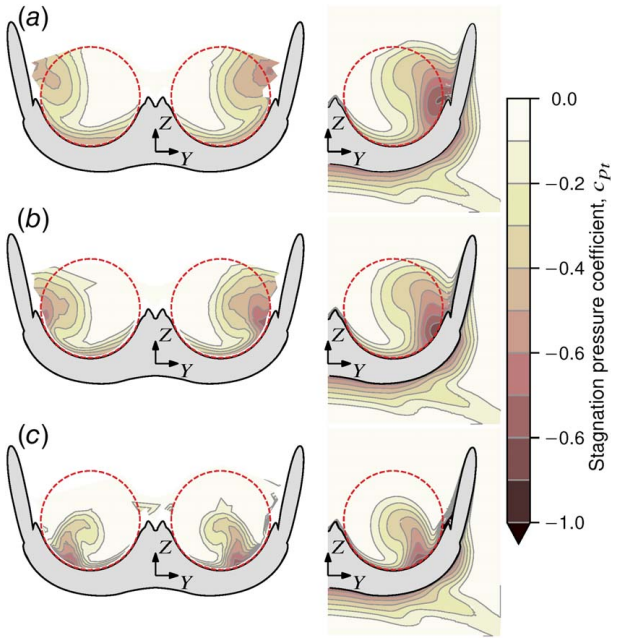

Fig. 14 Effect of propulsor power level on inlet stagnation pressure distortion: measured (left) and computed (right) inlet stagnation pressure coefficient at $\alpha = 8$ deg: (*a*) low power, (*b*) cruise power, and (*c*) high power

Downloaded from http://asmedigitalcollection.asme.org/turbomachinery/article-pdf/144/10/101002/6870956/turbo_144_10_101002.pdf by Massachusetts Inst Of Tech. user on 09 September 2022

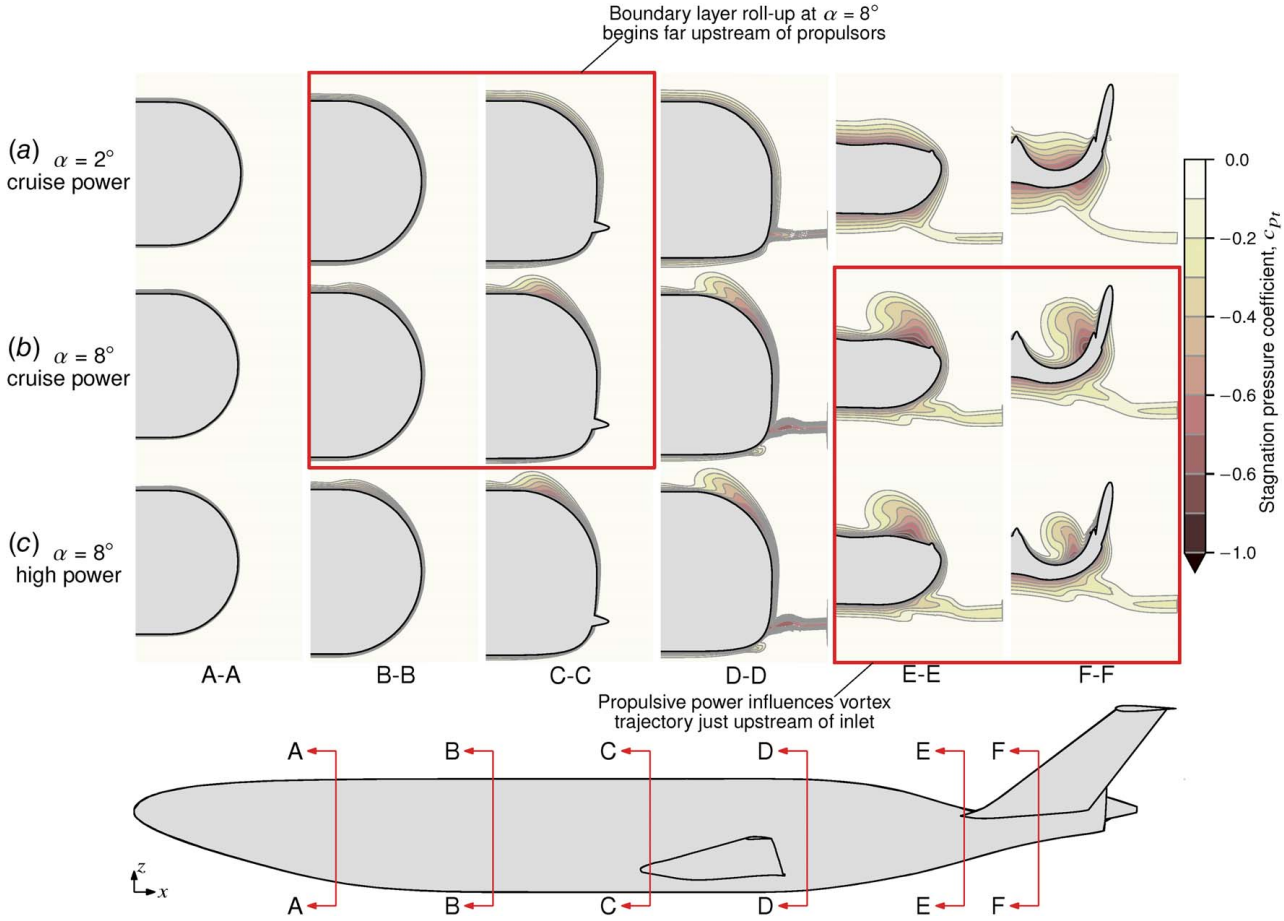

Fig. 15 Streamwise evolution of fuselage boundary layer stagnation pressure coefficient: (*a*) simulated cruise condition, (*b*) high angle of attack at cruise power, and (c) high angle of attack at high power

examine the effect of propulsor power on inlet distortion at 8 deg angle of attack (the points at high C_Z in Fig. 5). Figure 14 shows the measured and computed inlet stagnation pressure coefficient distributions at power levels near the high and low C_X corners of the wind tunnel model operating envelope and, for reference, the cruise power level. Again there is good qualitative agreement between measurements and computations; the largest quantitative differences are evident for the high power case, for which the discrepancy in overall force was largest (see Fig. 5), and for which, in the experiments, it was necessary to run the wind tunnel at a velocity half of that for the simulated cruise condition to achieve sufficiently high nondimensional fan speed, increasing the probe error by a factor of four.

Both the measurements and computations imply a large-scale vortex structure near the outboard boundary of the propulsor. As the fan power level, and thus the propulsor mass flow, increases, the vortex structure moves inboard from near the vertical tails toward the propulsor centerlines. As with changes in the angle of attack, changes in the propulsive power affect mainly the shape and location of the stagnation pressure distribution, rather than the magnitude of the stagnation pressure loss.

4.3 Streamwise Evolution of the Stagnation Pressure Field. The qualitative agreement between the measured and computed inlet distortions in Figs. 13 and 14 suggests that the computations correctly describe the upstream processes that generate the distortion. We can thus examine the computed flow field for these conditions at locations other than the measurement plane to gain better insight into the evolution of the stagnation pressure distribution upstream of the propulsor and connect the features of the fan inlet conditions to physical mechanisms. To this end, Fig. 15 shows the stagnation pressure coefficient distributions at axial locations along the fuselage for three different conditions: simulated cruise ($\alpha = 2$ deg) and high angle of attack ($\alpha = 8$ deg) at cruise fan power, and high angle of attack ($\alpha = 8$ deg) at high power.

At the simulated cruise condition (Fig. 15(*a*)), the boundary layer growth is close to uniform over the top half of the fuselage, with no indication of separation or streamwise vorticity. Comparison between the cruise condition and the case at 8 deg angle of attack at the same power level (Fig. 15(*b*)) shows that, in the latter, the low stagnation pressure fluid leaves the fuselage and starts to roll-up into a vortical structure with streamwise vorticity. This roll-up of the separated fuselage boundary layer starts forward of the wing leading edge, outside the influence of the fan. Comparison between high and low power conditions at 8 deg angle of attack shows the roll-up starting at the same location forward of the wing leading edge, with similar downstream development until just upstream of the inlet.

From these observations, we conclude that the change in inlet distortion, from a vertically stratified boundary layer flow to a large-scale streamwise vortex, arises not from fan-distortion interaction, but it is a feature of the lifting fuselage at the increased angle of attack. The influence of the propulsor, as stated previously, is largely a function of the fan mass flow, which determines the upstream area of the ingested streamtube and influences the trajectory of the ingested flow structures in the near field. This aspect of the inlet stagnation pressure distortion is accurately described in the computations, even with the uniform fan pressure rise approximation.

4.4 Inlet Streamwise Vorticity Distributions. Much of the distortion literature is concerned with stagnation pressure defects in an essentially unidirectional flow, but the measurements and

Downloaded from http://asmedigitalcollection.asme.org/turbomachinery/article-pdf/144/10/101002/6870956/turbo_144_10_101002.pdf by Massachusetts Inst Of Tech. user on 09 September 2022

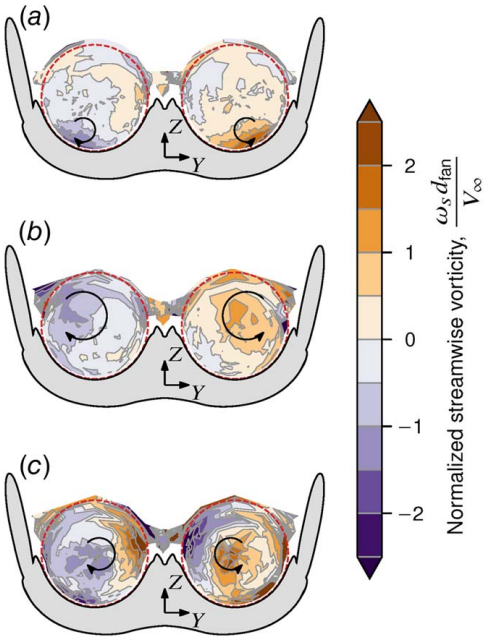

Fig. 16 Measured inlet plane-normal (streamwise) vorticity: (*a*) simulated cruise condition, (*b*) α = 8 deg at low power, and (*c*) α = 8 deg at high power

computations here show that the distortion of interest has an additional feature, the generation of streamwise vorticity, and the presence of swirl. Figure 16 shows measured distributions of nondimensional vorticity normal to the measurement plane, i.e., approximately streamwise vorticity, at three conditions. The vorticity was calculated via numerical differentiation of a linear interpolation of the data on the two-dimensional plane, introducing numerical noise in addition to the measurement uncertainty; however, overall trends in the magnitude and distribution of the vorticity are clear.

At the simulated cruise condition (Fig. 16(*a*)), the largest streamwise vorticity is concentrated at the bottom of the ingested boundary layer, consistent with the flow angularity observed in Fig. 6(*d*) and the surface streamline patterns in Fig. 8. As the angle of attack is increased, to 6 and 8 deg (not shown), the boundary layer fluid rolls up into a discrete vortex, and the location of maximum vorticity in the boundary layer moves outboard, following the trajectory of the region of minimum stagnation pressure in Fig. 13. Variations in the power level at 8 deg angle of attack (Figs. 16(*b*) and 16(*c*)) demonstrate that increasing the power increases the vorticity because the vortex lines are stretched, and the discrete vortex structure thus becomes more concentrated.

The vorticity distributions imply substantial transverse velocity components, and these impact fan rotor incidence distributions. The average vorticity over the inlet is mostly antisymmetric, which, coupled with co-rotating fans, results in differences between the fans, as discussed previously. Regions of locally high vorticity, on the other hand, may lead to increased circumferential or radial velocity nonuniformity. The vorticity distributions are consistent with the behavior, suggested based on the stagnation pressure data, of the fuselage boundary layer rolling up into discrete structures ingested by the propulsors at high angles of attack; the resulting three-dimensional velocity fields have different circumferential and radial nonuniformities at different operating conditions, which may have a strong impact on propulsor turbomachinery performance.

4.5 Integral Distortion Metrics. The discussion so far has focused on the physical features of BLI-associated distortion at different aircraft operating conditions. To quantify the severity of the distortion across these conditions and to make connection with distortion arising from causes other than BLI, we characterize the distortions in terms of DC(60), an industry standard metric for inlet circumferential distortion intensity [19]:

$$\mathrm{DC}(60) = \frac{\overline{p_t}|_{360\,\mathrm{deg}} - \overline{p_t}|_{\mathrm{worst}\,60\,\mathrm{deg}}}{\frac{1}{2}\rho V_x^2} \tag{1}$$

where $\overline{p_t}|_{360\,\mathrm{deg}}$ is the area-averaged stagnation pressure over the full annulus, $\overline{p_t}|_{\mathrm{worst}\,60\,\mathrm{deg}}$ is the lowest area-average over a 60-degree sector, and $\frac{1}{2}\rho V_x^2$ is the dynamic pressure based on the mean velocity.

Table 1 Measured inlet DC(60) for various simulated D8 mission operating conditions

Condition	α	$\Omega r_{tip}/V_\infty$	DC(60) (L)	DC(60) (R)
High α, idle	8 deg	1.28	0.437	0.617
Increased α	6 deg	2.71	0.442	0.479
Cruise	2 deg	2.70	0.390	0.442
High α	8 deg	2.71	0.342	0.454
Top of climb	2 deg	3.30	0.281	0.310
Start of climb	8 deg	5.70	0.132	0.142

Table 1 gives values of DC(60) for the different conditions. Results are shown for both the right and left propulsors because of the difference in operating point between the two (see Sec. 3.1). The results are ordered from largest to smallest average DC(60) between the two propulsors. The condition with the smallest DC(60) is the one with the highest vorticity (see Fig. 16(*c*)); conversely, the case with the largest DC(60) has the smallest peak vorticity (albeit with moderate values over the entire inlet, see Fig. 16(*b*)). These results highlight the fact that information about circumferential variations in stagnation pressure alone is not sufficient to describe the three-dimensional flow in BLI propulsors.

DC(60) has been used to correlate losses in compressor surge margin for different magnitudes and extents of distortion. There are, however, two important differences between its application in that venue and the present context. First, the stagnation pressure distortions that give rise to the correlations have been mainly unidirectional stagnation pressure defects. Second, the metric has been stall margin. In the present case, the distortions have both stagnation pressure defects and swirl and so refer to a qualitatively different type of flow. Further, a critical metric for BLI is the decrease in efficiency due to distortion, which is present even at the design condition, rather than the stall margin. The point is that DC(60) is used out of context and should not be considered a surrogate for characterizing effects of BLI on propulsor fan efficiency; this conclusion applies to other distortion descriptors based on circumferential variations in stagnation pressure (see, e.g., Ref. [30]).

The aforementioned arguments imply to us that the development of distortion metrics that directly indicate BLI fan efficiency changes would be a useful research area. Definition of such metrics is beyond the scope of the current effort, but we can suggest appropriate attributes based on our observations. Metrics used for correlation to fan efficiency should describe the nonuniformities that affect blade profile loss, namely, incidence angle and Mach number. Further, the nonuniformities should be captured on a per-ring basis, similar to the ARP1420 metrics [30], to account for radial variations in distortion. Finally, the metrics should describe not only local rotor loading but also give indication of any potential impacts of redistribution through the fan blade row, distortion fed to downstream guide vanes, and alterations in propulsor exit velocity.

5 Summary and Conclusions

First-of-a-kind in situ measurements of propulsor inlet and exit flow, as well as overall vehicle performance assessments, have been carried out for a 1:11-scale model of the D8 boundary layer ingesting (BLI) aircraft, with turbofan propulsors simulated by

Downloaded from http://asmedigitalcollection.asme.org/turbomachinery/article-pdf/144/10/101002/6870956/turbo_144_10_101002.pdf by Massachusetts Inst Of Tech. user on 09 September 2022

electric ducted fans, at the NASA Langley 14- by 22-foot Subsonic Tunnel. Complementary CFD computations connect the measurements to the overall vehicle flow field. The measurements and computations, obtained for a range of aircraft angles of attack and propulsive power settings, provide insight into the features of the fan inlet distortion due to BLI over the course of a typical flight profile, including qualitative and quantitative information about both the types of distortions encountered and the mechanisms responsible for their generation.

The results show there are three mechanisms that determine BLI propulsor inlet conditions. The first two, reduced stagnation pressure in the ingested boundary layer and the generation of streamwise vorticity through the rolling up of the fuselage boundary layer, are external flow features set by the aircraft angle of attack. The third mechanism, fan-distortion interaction, can be conceptually divided into far-field and near-field effects. In the far-field, the mass flow of the propulsor, i.e., the one-dimensional fan behavior, determines the streamtube capture area far upstream and the bulk trajectory of the ingested flow features. In the near-field, however, the three-dimensional effects associated with the nonuniform response of the fan to the incoming distortion result in axial velocity nonuniformity attenuation and associated swirl generation upstream of the fan. Comparison of the experimental and numerical results shows a uniform pressure rise actuator disk describes the far-field effects of BLI, but a higher-fidelity model is required to describe the near-field interactions and distortion transfer across the fan.

The measured distortions have been characterized in terms of DC(60), a commonly used inlet stagnation pressure distortion metric, allowing the comparison of distortion severity between operating conditions. Based on comparison with the fan inlet flow field, however, we find such metrics alone are inadequate for estimating the effects of BLI on fan performance, since they do not capture nonuniformities in axial and swirl velocities.

Acknowledgment

This work was supported by the NASA Fundamental Aeronautics Program Fixed Wing Project under Cooperative Agreement NNX11AB35A. It is a pleasure to acknowledge not only the funding but also the strong support rendered by, and the engagement in the project of the NASA program management team, especially Ruben Del Rosario, Kimlan Pham, and Richard Wahls. Preparation of this article was supported in part by NASA under award number 80NSSC19M0125 as part of the Center for High-Efficiency Electrical Technologies for Aircraft (CHEETA). We also wish to acknowledge the many helpful suggestions and other input by our colleagues. At MIT, these were (in alphabetical order) Cécile Casses, Arthur Huang, Tommy Li, Bob Liebeck, Michael Lieu, Nina Siu, Neil Titchener, and Elise van Dam. At Aurora Flight Sciences, this was Jeremy Hollman. At United Technologies Corporation, these were Alan Epstein, Wesley Lord (Pratt & Whitney) and Greg Tillman (United Technologies Research Center). At NASA Langley Research Center, these were Scott Anders, Greg Gatlin, and Judy Hannon. At NASA Ames Research Center, these were Dogus Akaydin and Tim Sandstrom. Finally, it is appropriate to conclude the acknowledgments by highlighting the exceptional support and level of professionalism of the staff at the NASA Langley 14- by 22-Foot Subsonic Tunnel, especially the two lead test engineers, Les Yeh (2013 tunnel entry) and Jim Byrd (2014 tunnel entry).

Conflict of Interest

There are no conflicts of interest.

Nomenclature

p = static pressure
c_p = static pressure coefficient $\left((p - p_\infty)/\left(\frac{1}{2}\rho V_\infty^2\right)\right)$
c_{pt} = stagnation pressure coefficient $\left((p_t - p_{t\infty})/\left(\frac{1}{2}\rho V_\infty^2\right)\right)$
d_{fan} = fan diameter
p_t = stagnation pressure
r_{tip} = fan tip radius
C_X = streamwise force coefficient
C_Z = stream-normal force coefficient
F_X = net streamwise aerodynamic force
F_Z = total (vertical) stream-normal aerodynamic force
S_{ref} = wing reference area
V_∞ = freestream velocity magnitude
y^+ = dimensionless wall distance
x, y, z = body Cartesian coordinate axes
DC(60) = distortion coefficient (60 deg distortion sector)
V_X, V_Y, V_Z = tunnel frame Cartesian velocity components
X, Y, Z = tunnel and freestream Cartesian coordinate axes

Greek Symbols

α = aircraft angle of attack
ρ = density
ω_s = streamwise vorticity
Ω = fan angular rotation rate

References

[1] Smith, L. H., 1993, "Wake Ingestion Propulsion Benefit," AIAA J. Propul. Power, **9**(1), pp. 74–82.
[2] Hall, D. K., Huang, A. C., Uranga, A., Greitzer, E. M., Drela, M., and Sato, S., 2017, "Boundary Layer Ingestion Propulsion Benefit for Transport Aircraft," AIAA J. Propul. Power, **33**(5), pp. 1118–1129.
[3] Drela, M., 2009, "Power Balance in Aerodynamic Flows," AIAA J., **47**(7), pp. 1761–1771.
[4] Uranga, A., Drela, M., Hall, D. K., and Greitzer, E. M., 2018, "Analysis of the Aerodynamic Benefit From Boundary Layer Ingestion for Transport Aircraft," AIAA J., **56**(11), pp. 4271–4281.
[5] Uranga, A., Drela, M., Greitzer, E. M., Hall, D. K., Titchener, N. A., Lieu, M. K., Siu, N. M., et al., 2017, "Boundary Layer Ingestion Benefit of the D8 Transport Aircraft," AIAA J., **55**(11), pp. 3693–3708.
[6] Seitz, A., Bijewitz, J., and Kaiser, S., 2014, "Conceptual Investigation of a Propulsive Fuselage Aircraft Layout," Aircr. Eng. Aerosp. Technol.: Int. J., **86**(6), pp. 464–472.
[7] Welstead, J. R., and Felder, J. L., 2016, "Conceptual Design of a Single-Aisle Turboelectric Commercial Transport With Fuselage Boundary Layer Ingestion," 54th AIAA Aerospace Sciences Meeting, AIAA Paper No. 2016-1027.
[8] Liebeck, R. H., 2004, "Design of the Blended Wing Body Subsonic Transport," AIAA J. Aircr., **41**(1), pp. 10–25.
[9] Hall, C. A., and Crichton, D., 2006, "Engine Design Studies for a Silent Aircraft," ASME J. Turbomach., **129**(3), pp. 479–487.
[10] Greitzer, E. M., Bonnefoy, P. A., Dorbian, C. S., Drela, M., Hall, D. K., Hansman, R. J., Hileman, J. I., et al., 2010, "N+3 Aircraft Concept Designs and Trade Studies, Final Report," NASA, Washington, DC, Report No. NASA CR-2010-216794.
[11] Drela, M., 2011, "Development of the D8 Transport Configuration," 29th AIAA Applied Aerodynamics Conference, AIAA Paper No. 2011-3970.
[12] Florea, R. V., Matalanis, C., Hardin, L. W., Stucky, M., and Shabbir, A., 2015, "Parametric Analysis and Design for Embedded Engine Inlets," AIAA J. Propul. Power, **31**(3), pp. 843–850.
[13] Wiart, L., Atinault, O., Paluch, B., Hue, D., and Grenon, R., 2015, "Development of NOVA Aircraft Configurations for Large Engine Integration Studies," 33rd AIAA Applied Aerodynamics Conference, AIAA Paper No. 2015-2254.
[14] Provenza, A. J., Duffy, K. D., and Bakhle, M. A., 2019, "Aeromechanical Response of a Distortion-Tolerant Boundary Layer Ingesting Fan," ASME J. Eng. Gas Turbines Power, **141**(1), p. 011011.
[15] Gunn, E. J., and Hall, C. A., 2014, "Aerodynamics of Boundary Layer Ingesting Fans," ASME Turbo Expo 2014: Turbine Technical Conference and Exposition, ASME Paper No. GT2014-26142.
[16] Ochs, S. S., Tillman, G., Joo, J., and Voytovych, D. M., 2017, "Computational Fluid Dynamics-Based Analysis of Boundary Layer Ingesting Propulsion," AIAA J. Propul. Power, **33**(2), pp. 522–530.
[17] Perovic, D., Hall, C. A., and Gunn, E. J., 2019, "Stall Inception in a Boundary Layer Ingesting Fan," AMSE J. Turbomach., **141**(9), p. 091007.
[18] Stenning, A. H., 1980, "Inlet Distortion Effects in Axial Compressors," ASME J. Fluid Eng., **102**(1), pp. 7–13.
[19] Longley, J. P., and Greitzer, E. M., 1992, "Inlet Distortion Effects in Aircraft Propulsion System Integration," Steady and Transient Performance Prediction of Gas Turbine Engines, AGARD Lecture Series, Vol. 183, Advisory Group for Aerospace Research and Development, Neuilly sur Seine, France.

Downloaded from http://asmedigitalcollection.asme.org/turbomachinery/article-pdf/144/10/101002/6870956/turbo_144_10_101002.pdf by Massachusetts Inst Of Tech. user on 09 September 2022

[20] Hall, D. K., Greitzer, E. M., and Tan, C. S., 2017, "Analysis of Fan Stage Conceptual Design Attributes for Boundary Layer Ingestion," ASME J. Turbomach., **139**(7), p. 071012.
[21] Uranga, A., Greitzer, E. M., Casses, C., DiOrio, A., Espitia, A., Grasch, A., Hall, D. K., et al., 2018, "Aircraft Technology Concepts for an N+3 Subsonic Transport, Phase 2 Final Report," MIT Gas Turbine Laboratory, Cambridge, MA, Report No. 2-001.
[22] Nichols, R. H., and Buning, P. G., 2021, "User's Manual for OVERFLOW 2.3," NASA, https://overflow.larc.nasa.gov/users-manual-for-overflow-2-3/, Accessed January 14, 2022.
[23] Pulliam, T. H., and Chaussee, D. S., 1981, "A Diagonal Form of An Implicit Approximate Factorization Algorithm," J. Comput. Phys., **39**(2), pp. 347–363.
[24] Menter, F. R., 1994, "Two-Equation Eddy-Viscosity Turbulence Models for Engineering Applications," AIAA J., **32**(8), pp. 1598–1605.
[25] Pandya, S. A., 2012, "External Aerodynamics Simulations for the MIT D8 'Double-Bubble' Aircraft Design," International Conference on Computational Fluid Dynamics, Vol. 7, Paper No. ICCFD7-4304.
[26] Pandya, S. A., Huang, A., Espitia, A., and Uranga, A., 2014, "Computational Assessment of the Boundary Layer Ingesting Nacelle Design of the D8 Aircraft," 52nd AIAA Aerospace Sciences Meeting, AIAA Paper No. 2014-0907.
[27] Defoe, J. J., and Spakovszky, Z. S., 2013, "Effects of Boundary-Layer Ingestion on the Aero-Acoustics of Transonic Fan Rotors," ASME J. Turbomach., **135**(5), p. 051013.
[28] Siu, N. M., 2015, "Evaluation of Propulsor Aerodynamic Performance for Powered Aircraft Wind Tunnel Experiments," M.S. thesis, Massachusetts Institute of Technology, Cambridge, MA.
[29] Hall, D. K., and Lieu, M. K., 2021, "Propulsor Models for Computational Analysis of Aircraft Aerodynamic Performance With Boundary Layer Ingestion," AIAA SciTech 2021 Forum, AIAA Paper No. 2021-0991.
[30] Aerospace Recommended Practice, 2017, "Gas Turbine Engine Inlet Flow Distortion Guidelines," SAE International, Aerospace Recommended Practice, Document ARP1420C.

Downloaded from http://asmedigitalcollection.asme.org/turbomachinery/article-pdf/144/10/101002/6870956/turbo_144_10_101002.pdf by Massachusetts Inst Of Tech. user on 09 September 2022